EUROFUSION WPCD-PR(16) 14920

G Fogaccia et al.

# Linear benchmarks between the hybrid codes HYMAGYC and HMGC to study energetic particle driven Alfvenic modes

Preprint of Paper to be submitted for publication in
Nuclear Fusion

This work has been carried out within the framework of the EUROfusion Consortium and has received funding from the Euratom research and training programme 2014-2018 under grant agreement No 633053. The views and opinions expressed herein do not necessarily reflect those of the European Commission.

# Linear benchmarks between the hybrid codes HYMAGYC and HMGC to study energetic particle driven Alfvénic modes

**G. Fogaccia, G. Vlad, S. Briguglio**

ENEA for EUROfusion, Frascati, (Rome) Italy

E-mail: giuliana.fogaccia@enea.it

**Abstract.** Resonant interaction between energetic particles (EPs) produced by fusion reactions and/or additional heating systems can destabilize global Alfvénic modes enhancing the EP transport. In order to investigate the EP transport in present and next generation fusion devices, numerical simulations are recognized as a very important tool. Among the various numerical models, the hybrid MHD gyrokinetic one has shown to be a valid compromise between a sufficiently accurate wave-particle interaction description and affordable computational resource requirements. This paper presents a linear benchmark between the hybrid codes HYMAGYC and HMGC. The HYMAGYC code solves the full, linear MHD equations in general curvilinear geometry for the bulk plasma and describes the EP population by the nonlinear gyrokinetic Vlasov equation. On the other side, HMGC solves the nonlinear, reduced $O(\epsilon_0^3)$, pressureless MHD equations ($\epsilon_0$ being the inverse aspect ratio) for the bulk plasma and the drift kinetic Vlasov equation for the EPs. The results of the HYMAGYC and HMGC codes have been compared both in the MHD limit and in a wide range of the EP parameter space for two test cases (one of which being the so-called TAE $n = 6$ ITPA Energetic Particle Group test case), both characterized by $\epsilon_0 \ll 1$.

PACS numbers: 52.35.Bj, 52.35.Py, 52.55.Pi, 52.65.Ww, 52.30.Cv, 52.30.Cz, 52.55.Tn, 52.65.Rr

Submitted to: *Nuclear Fusion*

## 1. Introduction

One of the major challenges to be met in the magnetic confinement thermonuclear fusion research concerns the confinement, inside the reaction chamber of a burning plasma, of the energetic particles (EPs) produced by fusion reactions ($\alpha$ particles). Fusion $\alpha$ particles have velocities of the order of Alfvén velocity (the propagation velocity of a shear Alfvén wave). Then, they can resonantly interact with the shear Alfvén waves, driving global modes (e.g. TAE [1, 2], KTAE [3], EPM [4],...) which, in turn, could enhance the EP transport toward the first wall and lead to a significant particle and heat loading. In the present day experiments, resonant destabilization of global Alfvén modes by EPs, produced by additional heating systems as Electron and Ion Cyclotron Resonant Heating (ECRH and ICRH) and Neutral Beam Injection (NBI), have been widely observed [5, 6, 7, 8]. In order to predict and, eventually, minimize the EP transport in the next generation fusion devices, several numerical models have been developed, based on different theoretical approaches: gyrofluid codes [9], extended, kinetic MHD codes [10, 11, 12, 13, 14, 15, 16], hybrid MHD gyrokinetic codes [17, 18, 19, 20, 21, 22, 23, 24, 25, 26] and fully gyrokinetic codes [27, 28, 29].

Among them, the hybrid model has shown to be a valid compromise between a sufficiently accurate wave-particle interaction description and affordable computational resource requirements. The hybrid model describes some components of the plasma using Magnetohydrodynamics (MHD) equations, treating the others through the nonlinear gyrokinetic Vlasov equation (see [30] and references therein). In the present paper, linear benchmarks between the two hybrid codes HYMAGYC [31] and HMGC [18, 20] are presented. Both codes describe thermal (bulk) plasma as a single fluid, by MHD equations; EPs are described in terms of their distribution function by nonlinear gyrokinetic Vlasov equation. They are self-consistent codes: that is, at each time step, the divergence of the EP pressure tensor is computed in the gyrokinetic (GK) module and returned to the MHD one (the "field solver"), which computes the new electromagnetic fields in which EPs will move in the next time step. The nonlinear gyrokinetic Vlasov equation is solved for both codes in the GK module by particle-in-cell (PIC) techniques.

The HYMAGYC code [31] is a recently developed HYbrid MAgnetohydrodynamics GYrokinetic Code suitable to study EP driven Alfvénic modes in general high-$\beta$ axisymmetric equilibria, (with $\beta$ being the ratio of the plasma pressure to the magnetic pressure), with perturbed electromagnetic fields (electrostatic potential $\phi$ and vector potential $\mathbf{A}$) fully accounted for. The thermal plasma is described by linear full resistive MHD equations in arbitrary axisymmetric equilibria. The MHD field solver relies on equilibrium quantities computed by the equilibrium code CHEASE [32] (as, e.g., covariant and contravariant metric tensor coefficients, Jacobian, equilibrium magnetic field, current density components and pressure). It is also fully interfaced with the European Integrated Modelling Framework data structure [33] (formerly ITM, presently

maintained by the EU-IM Team‡). Such field solver originates from the code MARS [34], which has been transformed from an eigenvalue solver to an initial value one (see Appendix A.2 in [35]). The MARS kernel uses Fourier decomposition in generalized poloidal ($\chi$) and toroidal ($\varphi$) angles and generalized finite element method along with the Tunable Integration Method [36] for the discretization in the radial-like coordinate $s = \sqrt{|\psi_{eq} - \psi_0|/|\psi_{edge} - \psi_0|}$ (with $\psi_{eq}$ the equilibrium poloidal flux function, and $\psi_0$ and $\psi_{edge}$, respectively, the value of $\psi_{eq}$ on the magnetic axis and at the last closed magnetic surface). The EP population is described by the nonlinear gyrokinetic Vlasov equation, expanded up to order $\mathrm{O}(\epsilon^2)$ and $\mathrm{O}(\epsilon\epsilon_B)$, $\epsilon$ being the gyrokinetic ordering parameter $\epsilon \sim \rho_H/L_n$ and $\epsilon_B \sim \rho_H/L_B$, with $\rho_H$ the energetic ("hot") particle Larmor radius, $L_n$ and $L_B$ the characteristic equilibrium plasma density and magnetic-field nonuniformity length scales, respectively. As $L_n/L_B \ll 1$, we neglect $\mathrm{O}(\epsilon_B^2)$ terms. The perturbed electromagnetic fields are assumed to be low-frequency fluctuations characterized by short wavelengths perpendicular to the equilibrium magnetic field and long wavelengths parallel to it. The following space-time ordering for the fluctuating electromagnetic fields holds [37]: $k_\perp \rho_H = O(1)$, $k_\parallel \rho_H = O(\epsilon)$, $\omega/\Omega_H = O(\epsilon)$, being $k_\perp$ the perpendicular (to the equilibrium magnetic field) wave vector of perturbed fields, $k_\parallel$ the parallel one, $\omega$ the characteristic fluctuation frequency and $\Omega_H = q_H B/m_H c$ the EP gyrofrequency, with $q_H$, $m_H$, $B$ and $c$ the EP charge, the EP mass, the equilibrium magnetic field and the light velocity, respectively. Flux coordinates system ($s$, $\chi$, $\varphi$) is used.

On the other side, HMGC describes the thermal plasma by nonlinear reduced $O(\epsilon_0^3)$ visco-resistive MHD equations, being $\epsilon_0 \equiv a/R_0$ the inverse of aspect ratio (with $a$ and $R_0$ the minor and major radius of the torus, respectively) evolving the fluctuating electrostatic field $\phi$ and the perturbed vector potential component, parallel to the equilibrium magnetic field, $A_\parallel$ (low-$\beta$ limit), in the zero pressure limit. The EP population is described by the nonlinear gyrokinetic Vlasov equation, in the $k_\perp \rho_H \ll 1$ limit (drift-kinetic limit). Note that HMGC is restricted to simple geometry, considering only equilibria with shifted circular magnetic surfaces. A toroidal coordinates system ($r$, $\theta$, $\varphi$), finite differences in the radial coordinate $r$ and Fourier decomposition in the poloidal $\theta$ and toroidal $\varphi$ coordinates are used. The divergence of the EP pressure tensor $\nabla \cdot \Pi_H$ to be fed in the MHD equations, in both codes, is treated as an explicit term in the time discretization scheme.

For the purpose of this benchmark exercise, the gyrokinetic equations implemented in HYMAGYC have been reduced to the drift-kinetic ones ($k_\perp \rho_H \ll 1$); moreover, $\delta A_\perp$ has been neglected, and a pressureless equilibrium with $\epsilon_0 \ll 1$ and circular poloidal cross section has been considered, in order to be consistent with the limits adopted in HMGC. Furthermore, the EP pressure tensor $\Pi^i_{j,H}$ has been diagonalized to reproduce that utilized in the HMGC model (here, $i, j$ stand for $s, \chi, \varphi$). Previous tests [38] have compared the single particle orbits in equilibrium fields and the evolution

‡ See http://www.euro-fusionscipub.org/eu-im

of the EP response of the GK modules of HYMAGYC and HMGC to a given perturbed electromagnetic fields. Here, we consider the comparison between HYMAGYC and HMGC for two test cases A and B, presented, respectively, in Sec.2 and Sec.3. Simulation results obtained by HMGC and HYMAGYC are compared in the MHD limit (Sec.2.1 and 3.1) and in the presence of EPs (Sec. 2.2 and 3.2), for both test cases.

## 2. Test case A

The first test case assumes a circular shifted magnetic-surface equilibrium characterized by a large aspect ratio ($\epsilon_0 = 0.1$) and a parabolic safety factor profile $q(r) = q_0 + (q_a - q_0)(r/a)^2$, $q_0 = 1.1$, $q_a = 1.9$, in the presence of a Maxwellian initial EP population. A bulk ion density profile $n_i \propto 1/q^2$ (such to have all the toroidal frequency gaps aligned) and a zero bulk plasma pressure (HMGC limit) are assumed. In order to ensure numerical stability in HMGC, a finite bulk plasma resistivity $\eta$ is necessary: in the following a value of resistivity corresponding to the inverse Lundquist number $S^{-1} = \eta R_0/(\mu_0 a^2 v_{A0}) = 10^{-6}$ is considered (with $v_{A0} \equiv B_0/\sqrt{4\pi m_i n_{i0}}$ the on-axis Alfvén velocity, $m_i$ and $n_{i0}$ the bulk ion mass and on-axis density). Equilibrium (initial) EP distribution function has been considered to be an isotropic Maxwellian, with a radial density profile $n_H = n_{H0}\exp(-19.53 s^4)$, $T_H/T_{H0} = 1$, $\rho_{H0}/a = 0.01$, $v_{H0}/v_{A0} = 1$, $m_H/m_i = 2$ ($T_{H0}$, $\rho_{H0}$ and $v_{H0}$ are the on-axis EP temperature, Larmor radius and thermal velocity, respectively). In Fig.1 the safety factor $q$ profile, the normalized bulk ion density $n_i/n_{i0}$ and the normalized EP density $n_H/n_{H0}$ profiles, used in the HMGC simulations, are plotted.

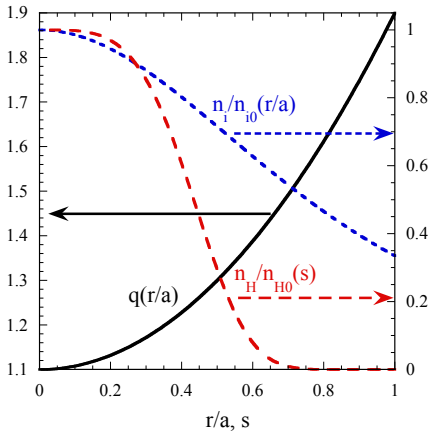


**Figure 1.** Test case A: safety factor $q$ profile (black curve) and normalized bulk ion density (dashed blue curve) vs $r/a$; normalized EP density $n_H/n_{H0}$ (dashed red curve) vs $s$.

The code HYMAGYC requires a high resolution Grad-Shafranov solver to compute a proper MHD equilibrium; for this benchmark we rely on CHEASE [32], which

**Table 1.** Test case A: MARS results (TAE and the first Upper and Lower Resistive Periodic Shear Alfvén Modes, RPSAEs).

| mode | $S^{-1}$ | $\omega/\omega_{A0}$ | $\gamma/\omega_{A0}$ |
|---|---|---|---|
| TAE | 0 | 0.4404 | $< 10^{-13}$ |
| TAE | $10^{-6}$ | 0.4404 | -0.000867 |
| Upper RPSAE | $10^{-6}$ | 0.483 | -0.00337 |
| Lower RPSAE | $10^{-6}$ | 0.42205 | -0.00803 |

requires as inputs, besides the shape of the last closed magnetic surface, the two free functions $p'(\psi_{eq})$ and $TT'(\psi_{eq})$ (here, $p(\psi_{eq})$ is the equilibrium plasma pressure, $T(\psi_{eq}) \equiv RB_\varphi$ denotes the poloidal current flux function, and prime denotes the derivative with respect to $\psi_{eq}$). For the chosen equilibrium, $p' = 0$, and $TT'(\psi_{eq})$ has been reconstructed from the Grad-Shafranov equation computing $\Delta^*\psi_{eq,HMGC}$ (here $\Delta^* \equiv R\,\partial/\partial R\,(1/R\,\partial/\partial R) + \partial^2/\partial Z^2$ is the so-called Shafranov operator, and $\psi_{eq,HMGC}$ is the poloidal magnetic flux function as obtained by the equilibrium solver for HMGC, which uses, as input, the radial profile of the safety factor $q$ defined above, see Appendix A.4 in [35]). A toroidal mode number $n = 2$, and poloidal harmonics $m = 1 - 4$ have been considered.

### *2.1. MHD limit*

The linear MHD stability of such equilibrium can be studied by the linear stability eigenvalue code MARS [34] from which the MHD field solver of HYMAGYC originates. Such equilibrium admits, in the ideal limit ($S^{-1} = 0$), a marginally stable TAE mode, located in frequency inside the toroidal gap at $\omega/\omega_{A0} \approx 0.44$ ($\omega_{A0} \equiv v_{A0}/R_0$ being the on-axis Alfvén frequency), and in radius at the position of the throats of the Alfvén continua (principally at the internal one, at $s \approx 0.5$, but also at the external one, at $s \approx 0.9$). In presence of finite resistivity the TAE mode becomes stable and global discrete stable modes appear also in the upper and lower continua (RPSAE [1, 35]) (see Table 1). The eigenfunctions determined by the MARS runs have been used as initial conditions for the MHD module of HYMAGYC. During simulations the spatial structure of each eigenfunction does not change, and only its amplitude decreases, because of the damping (see Fig. 2 for the results of the three resistive Alfvénic modes, $S^{-1} = 10^{-6}$). In Fig. 3 the dependence of the damping rate from the time step $dt$ used in the HYMAGYC simulations is shown, for the ideal and resistive ($S^{-1} = 10^{-6}$) TAE. Note that for $dt \to 0$ the damping rates tend to the values obtained by MARS (see the square symbols in Fig. 3 ). Unfortunately, HMGC does not have a "companion" eigensolver code (as it is MARS for HYMAGYC), and, thus, it is not easy to initialize a simulation to clearly follow in time the evolution of a specific stable eigenmode. To overcome this difficulty, an "antenna" like driving term has been added to HMGC in order to excite preferentially

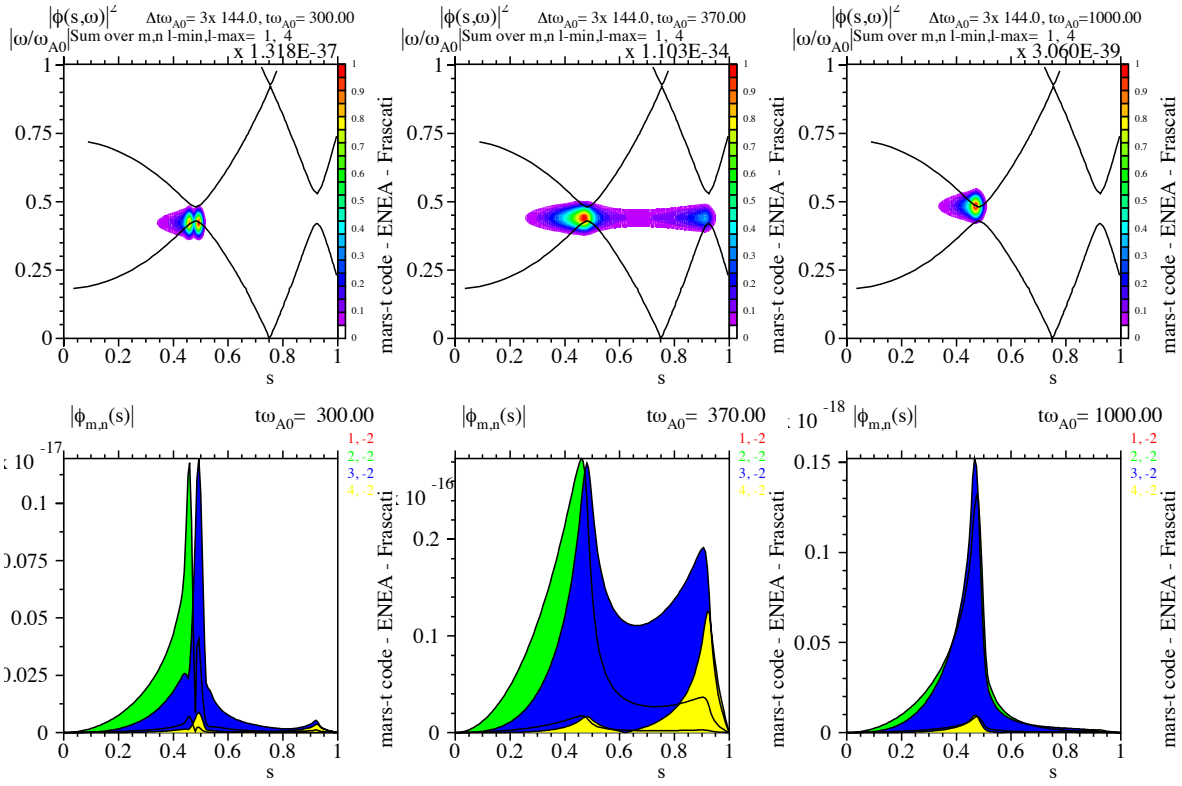


**Figure 2.** Test case A: frequency spectrum of the electrostatic potential $\phi$ (top) and its Fourier components (bottom) for the first Lower RPSAE (left), resistive TAE (center) and first Upper RPSAE (right), $S^{-1} = 10^{-6}$; fill colors refer to different $m$'s (1: red, 2: green, 3: blue, 4: yellow).

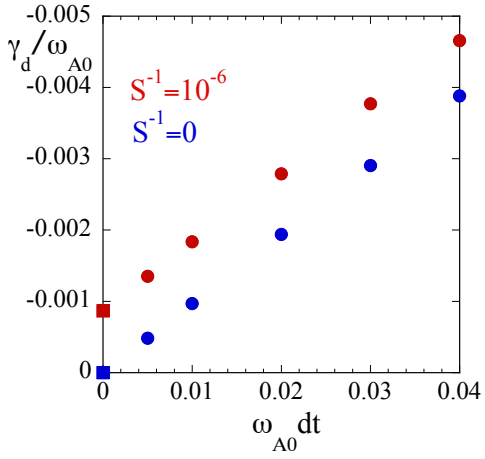


**Figure 3.** Test case A: damping rate $\gamma_d$ vs. $dt$ for ideal (blue symbols) and resistive ($S^{-1} = 10^{-6}$, red symbols) TAE, using the MHD module of HYMAGYC for $dt \neq 0$ (circle symbols) and the eigenvalue code MARS for $dt = 0$ (square symbols).

a specific eigenfrequency, and, then, use the corresponding eigenfunction to initialize a "decay numerical experiment" case. The use of this procedure allows us to obtain damping rates also for HMGC, at least for the TAE and the Upper RPSAE mode (results for the Lower RPSAE are less clear, because of its larger damping, and, thus, are not reported here). In Fig. 4 the eigenvalues (real frequency and damping rate) so obtained by HMGC are compared with the ones obtained by HYMAGYC (vertical dashed lines refer to the lower and upper accumulation points of the Alfvén continua). From Fig. 4 it can be observed that the damping rates obtained by the MHD module

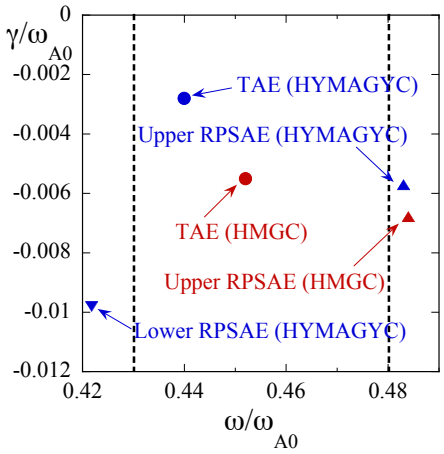


**Figure 4.** Test case A: eigenvalues obtained by HMGC (red symbols) and HYMAGYC (blue symbols), for $\omega_{A0}dt = 0.02$, $S^{-1} = 10^{-6}$.

of HMGC are larger than the corresponding ones obtained by HYMAGYC. Then the numerical scheme for time integration used in the MHD module of HMGC seems to be, generally speaking, more dissipative than the one used in in the MHD module of HYMAGYC.

In order to evaluate the effect of inserting in the MHD module of HYMAGYC the EP drive treated explicitly in the time integration scheme, a term $\propto \gamma_v \mathbf{X}$ (explicitly treated in the time discretization scheme) has been added to the MHD equations both for HYMAYGYC and for HMGC. Here, $\mathbf{X}$ is the full set of unknown fields, which, for HYMAGYC are the perturbed contravariant components of the plasma velocity and magnetic fields and the (scalar) pressure, and, in HMGC, the electrostatic potential $\phi$ and the parallel component of the vector potential $A_\parallel$; $\gamma_v$ is a numerical coefficient representing the drive intensity. Note that this term, being purely real, will not force the system to a (externally) given real frequency, but will drive the less damped (or most unstable) mode. Both codes behave similarly, being exited the same (TAE) mode and showing a similar slope of the curve $\gamma$ vs. $\gamma_v$ (see Fig.5), with $\gamma$ the growth rate of the TAE mode.

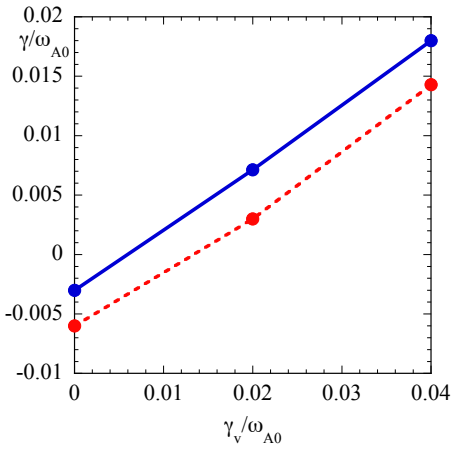


**Figure 5.** Test case A: growth rate of the TAE mode exited by an external drive vs. the drive intensity, for HMGC (red symbols) and HYMAGYC (blue symbols).

### *2.2. Results with energetic particle drive*

In the following, we compare the HYMAGYC code results w.r.t. the HMGC ones, in the presence of the EP drive ($n_{H0}/n_{i0} \neq 0$), restricting, in this paper, the comparison to the linear growth regime. Similar phenomenology is shown by the two codes. At low EP density, a mode in the upper Alfvén continuum, close to the toroidal gap, is destabilized ("Upper mode", Fig. 6), while, at higher density values, the most unstable mode lives deeply inside the lower Alfvén continuum (EPM mode, Fig. 7).

While the results of the two codes qualitatively compare fairly well w.r.t. real frequencies (see Fig. 8, bottom left), eigenfunctions (see Fig. 6 and Fig. 7, centre) and thresholds for the onset of the EPM (see Fig. 8, top left), some more quantitative differences are observed concerning the growth rates, in particular for the strongly driven EPM. Such consideration has suggested to test independently the GK module of HYMAGYC in the presence of MHD fields self-consistently computed by the MHD module used in HMGC (this "mixed" code version will be indicated, in the following, as "hymagyc-hmgc"). Note that the substitution of the GK module requires a new interface between the MHD module of HMGC and the GK module of HYMAGYC. Results for the two modes described above as obtained using "hymagyc-hmgc" are shown in Figs. 6, 7 (bottom). The agreement, for the two modes considered, is quite satisfactory, w.r.t. frequency spectra, radial profiles of the Fourier components of the eigenfunctions and their poloidal structures.

The growth-rates and real frequencies of the destabilized modes have been compared between HMGC, "hymagyc-hmgc" and HYMAGYC, varying independently the normalized on-axis EP density value $n_{H0}/n_{i0}$ (Fig. 8, left); similar scans varying the normalized on-axis EP thermal velocity $v_{H0}/v_{A0}$ and the normalized on-axis EP Larmor radius $\rho_{H0}/a$ as free parameters have also been done (Fig. 8, centre and right).

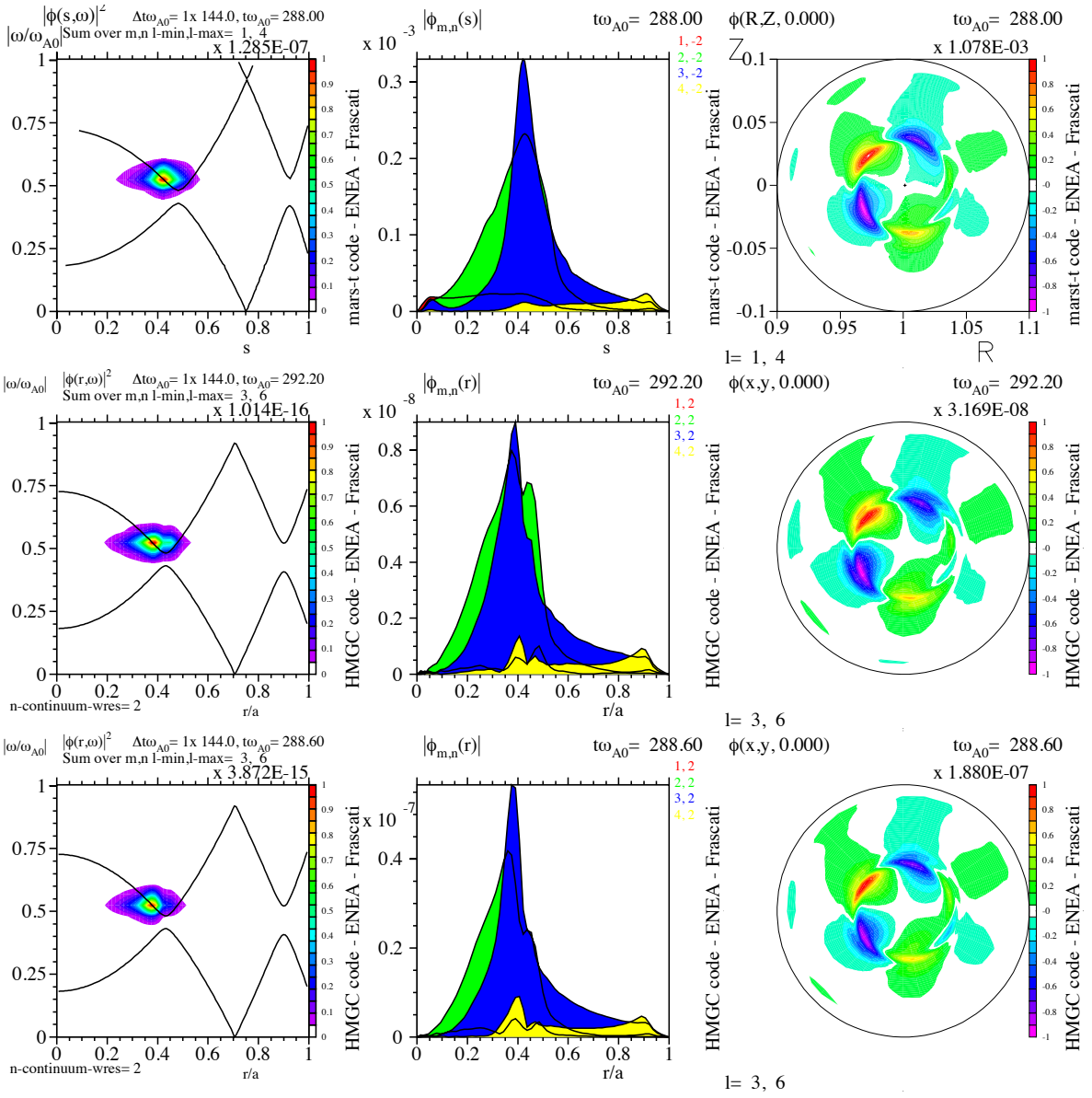


**Figure 6.** Test case A: Upper mode ($n_{H0}/n_{i0} = 1.75 \times 10^{-3}$). Results from HYMAGYC (top), HMGC (centre) and "hymagyc-hmgc" (bottom). The frequency spectrum of the fluctuating electrostatic potential $\phi$ (left), its poloidal Fourier components (centre), and its structure in the poloidal plane (right), are shown.

Quantitatively, frequencies observed in the HYMAGYC simulations are lower by 10% for the "Upper mode" and by 40% for the EPM, with respect to that obtained by HMGC code, whereas the growth rates observed in the HYMAGYC simulations are larger up to 50% than that obtained with the HMGC code. The "hymagyc-hmgc" code shows results very similar to that obtained from the HMGC code for the "Upper mode", while for the EPM mode it shows intermediate results between HYMAGYC and HMGC ones. Figure 9 shows, for the "Upper mode" as obtained by HYMAGYC and HMGC, the growth rate vs. $v_{H0}/v_{A0}$, varying accordingly $\rho_{H0}/a$ w.r.t. the reference values,

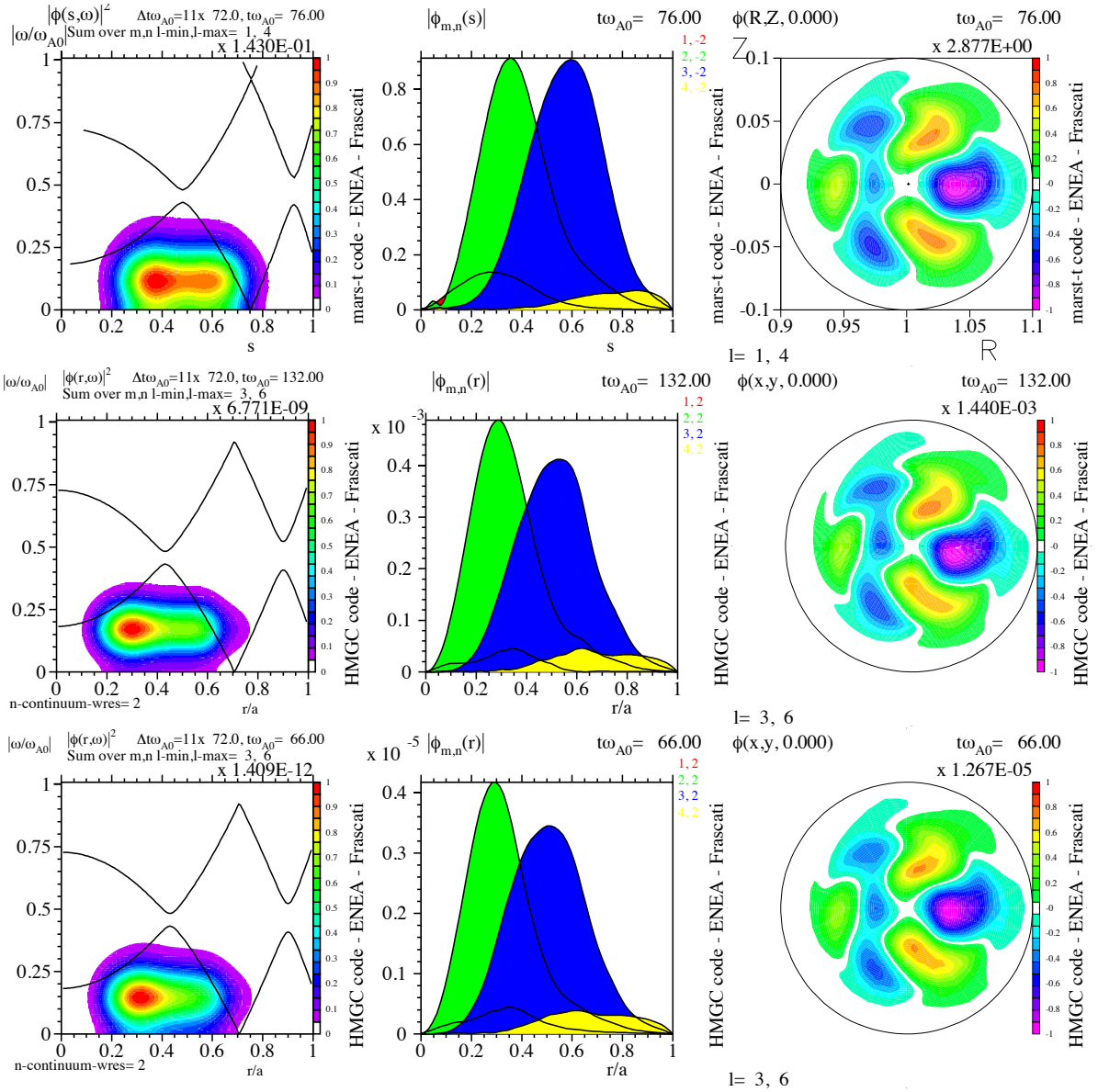


**Figure 7.** Test case A: EPM mode ($n_{H0}/n_{i0} = 3.75\times10^{-3}$): results from HYMAGYC (top), HMGC (centre) and "hymagyc-hmgc" (bottom). Frequency spectrum of the fluctuating electrostatic potential $\phi$ (left), its poloidal Fourier components (centre), and its structure in the poloidal plane (right), are shown.

while keeping fixed $\beta_{H0}$ (at the value $\beta_{H0} = 7.\times10^{-3}$, corresponding to the parameters $v_{H0}/v_{A0} = 1.$, $n_{H0}/n_{i0} = 1.75\times10^{-3}$): while the behaviour of the curves for HYMAGYC and HMGC is qualitatively in agreement, the absolute values differ considerably. In Fig. 9 it is also shown a point representing the EP drive $\gamma_{drive}$, valued by algebraically subtracting from the growth rate the $\gamma_{damping}$ estimated by extrapolating to $n_{H0}/n_{i0} = 0$ the growth rates shown in Fig. 8, top left ($v_{H0}/v_{A0} = 1.$). The discrepancy between the drives is smaller, thus suggesting that the differences between HYMAGYC and HMGC observed in the growth rates can be mainly traced back to the MHD damping (e.g.,

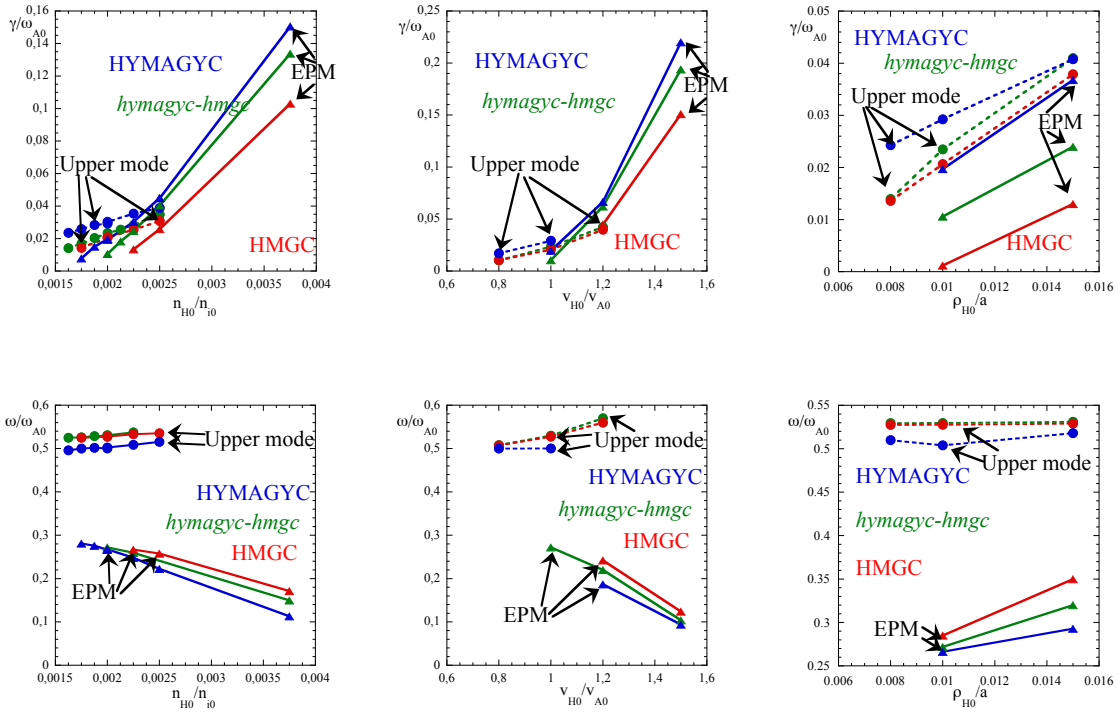


**Figure 8.** Test case A: normalized growth rates (top) and frequencies (bottom) versus: $n_{H0}/n_{i0}$ (left, with $v_{H0}/v_{A0} = 1.$ and $\rho_{H0}/a = 0.01$), $v_{H0}/v_{A0}$ (centre, with $n_{H0}/n_{i0} = 0.002$ and $\rho_{H0}/a = 0.01$) and $\rho_{H0}/a$ (right, with $n_{H0}/n_{i0} = 0.002$ and $v_{H0}/v_{A0} = 1.$). Results for HMGC (red symbols), HYMAGYC (blue symbols) and "hymagyc-hmgc" (green symbols) simulations are shown.

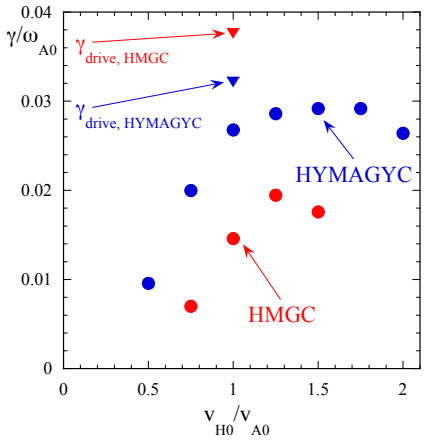


**Figure 9.** Test case A: normalized growth rates versus $v_{H0}/v_{A0}$. Results for HMGC (red symbols) and HYMAGYC (blue symbols) simulations are shown; the triangles at $v_{H0}/v_{A0} = 1.$ are the EP $\gamma_{drive}$.

continuum damping) and the numerical damping related to the discretization schemes.

## 3. Test case B

As a second benchmark for HYMAGYC, we have considered the case analyzed by the ITPA Energetic Particle Group, the so-called TAE, $n = 6$ case [39]. As before, the safety factor profile is parabolic, with $q_0 = 1.714$, $q_a = 1.87$ (i.e. with very small magnetic shear), $R_0 = 10m$, $a = 1m$ (thus, $\epsilon_0 = 0.1$), on-axis magnetic field $B_0 = 3T$, bulk plasma characterized by flat ion (Hydrogen) density $n_{i0} = 2 \times 10^{19} m^{-3}$, but still considering zero beta bulk plasma. EP (Deuterium) distribution function is Maxwellian, with $T_H = T_{H0} = 400keV$, $n_H(s) = n_{H0}\, c_3 \exp\left(-\frac{c_2}{c_1} \tanh \frac{s-c_0}{c_2}\right)$, with $c_0 = 0.49123$, $c_1 = 0.298228$, $c_2 = 0.198739$, and $c_3 = 0.521298$. The profiles of safety factor, normalized ion bulk and EP densities, used in the HMGC simulations, are shown in Fig.10.

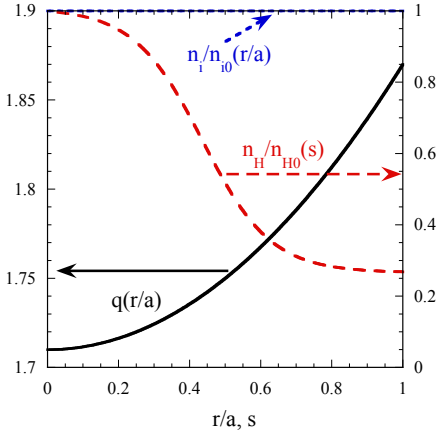


**Figure 10.** Test case B: safety factor $q$ profile (black curve) and normalized bulk ion density (dashed blue curve) vs $r/a$; normalized EP density $n_H/n_{H0}$ (dashed red curve) vs $s$.

Moreover, the nominal value used in the ITPA benchmark for the on-axis EP density is $n_{H0} = 1.44131 \times 10^{17} m^{-3}$, corresponding to $n_{H0}/n_{i0} = 7.20655 \times 10^{-3}$. These parameters yield $v_{H0}/v_{A0} \simeq 0.3$ and $\rho_{H0}/a \simeq 0.03$. Simulations for toroidal mode number $n = 6$ and poloidal harmonics $m = 8 - 13$ have been performed.

### *3.1. MHD limit*

A rich MHD spectrum (see Fig.11) has been found for this equilibrium around the toroidal frequency gap, by running at first the MHD linear stability eigenvalue code MARS, in the ideal and resistive cases. For $S^{-1} = 0$, two marginally stable TAE modes with $\omega/\omega_{A0} \approx 0.281$ and $\omega/\omega_{A0} \approx 0.302$ have been found (full blue circles);

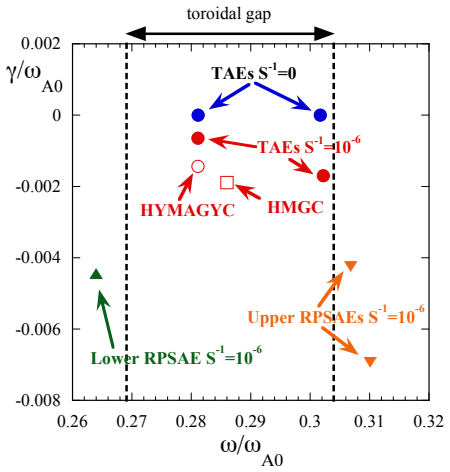


**Figure 11.** Test case B: eigenvalues obtained by MARS for $S^{-1} = 0$ (full blue circles) and $S^{-1} = 10^{-6}$ (full red circles, green and orange triangles), by HYMAGYC (empty red circle) and HMGC (empty red square) for $S^{-1} = 10^{-6}$.

for $S^{-1} = 10^{-6}$ such modes become stable (full red circles), with the TAE mode near the lower Alfvén continuum (left vertical dashed line in Fig.11) the less damped one, with $\gamma/\omega_{A0} \approx -0.000645$. Stable Lower and Upper RPSAE modes also appear (green and orange triangles, respectively). HYMAGYC and HMGC simulations have been performed in the MHD limit with $S^{-1} = 10^{-6}$; for HYMAGYC, mode structure has been initialized to the eigenfunction found by MARS for the TAE mode near the lower Alfvén continuum. Both codes show a more stable TAE (the total damping being due to the resistivity and to the numerical time integration scheme used from each code), characterized by $\omega/\omega_{A0} \approx 0.281$ and $\gamma/\omega_{A0} \approx -1.4354 \times 10^{-3}$ for HYMAGYC (empty red circle), and $\omega/\omega_{A0} \approx 0.286$, $\gamma/\omega_{A0} \approx -1.8894 \times 10^{-3}$ for HMGC (empty red square).

### *3.2. Results with energetic particle drive*

In order to test the linear growth phase of HMGC and HYMAGYC codes, the EP density has been varied (see Fig. 12) while keeping fixed $v_{H0}/v_{A0}$ and $\rho_{H0}/a$: at low values of $n_{H0}/n_{i0}$ (w.r.t. $n_{H0}/n_{i0} \approx 7.2 \times 10^{-3}$, the reference ITPA benchmark case value), frequencies and growth-rates obtained by the two codes are very similar, corresponding to a mode localized in the toroidal gap, i.e., a TAE (see Fig. 12, right, circle symbols); for higher values of $n_{H0}/n_{i0}$, on the contrary, the most unstable mode obtained by HYMAGYC is clearly a mode emerging from the lower Alfvén continuum, i.e., a lower KTAE (see Fig. 12, right, triangle symbols) which exhibits a stronger growth rate, w.r.t. the most unstable mode observed by HMGC, which is still a TAE. The different nature of the two modes are clearly observed in Fig. 13 and Fig. 14 which refer to HYMAGYC and HMGC simulations, for $n_{H0}/n_{i0} = 2 \times 10^{-3}$ and $n_{H0}/n_{i0} \approx 7.2 \times 10^{-3}$, respectively.

Note that also in the lower density case some differences regarding the symmetry

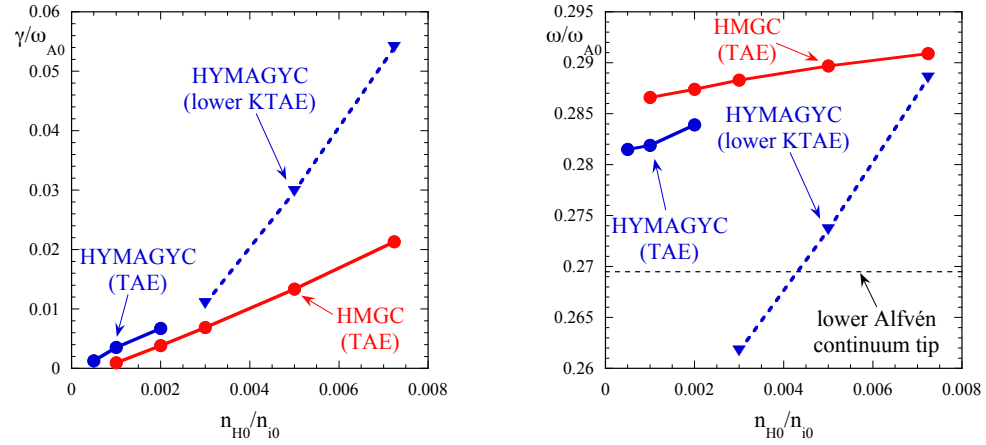


**Figure 12.** Test case B: normalized growth rates (left) and frequencies (right) versus $n_{H0}/n_{i0}$. Results for HMGC (red symbols) and HYMAGYC (blue symbols) simulations are shown, for the ITPA benchmark case. The dashed horizontal line in the right plot refer to the lower tip of the Alfvén continuum $\omega_{l.c.}/\omega_{A0} \approx 0.269$, the upper tip (not shown) being at $\omega_{u.c.}/\omega_{A0} \approx 0.310$.

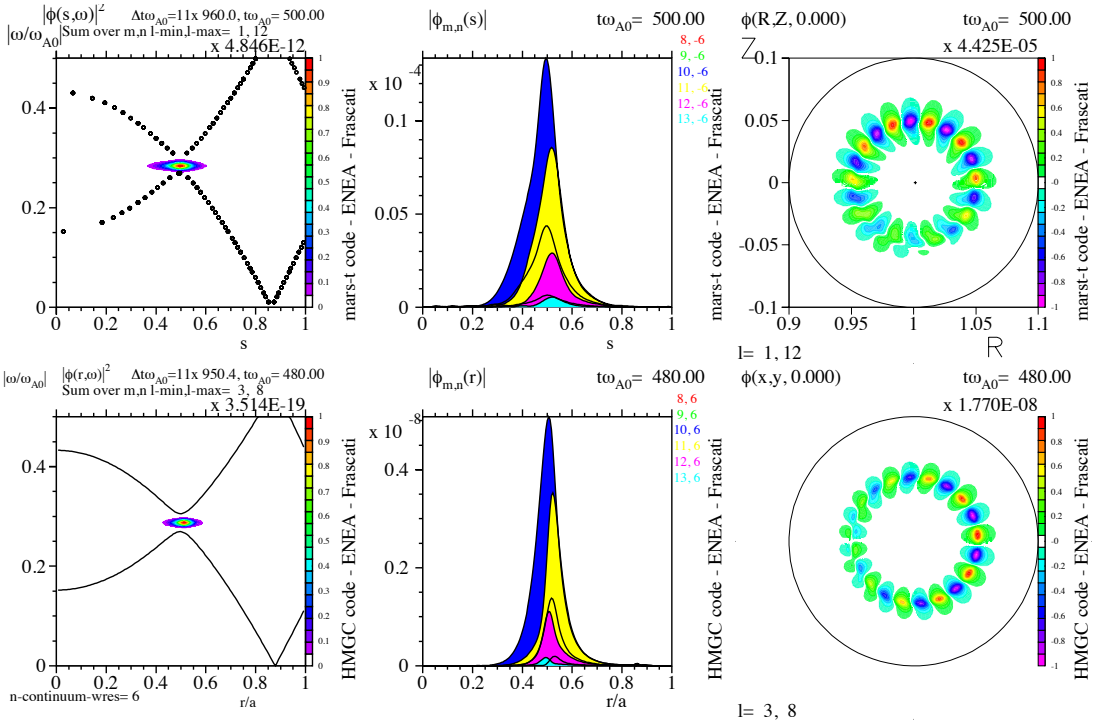


**Figure 13.** Test case B: results from HYMAGYC (top) and HMGC (bottom) for $n_{H0}/n_{i0} = 2 \times 10^{-3}$ (TAE). The frequency spectrum of the fluctuating electrostatic potential $\phi$ (left), its poloidal Fourier components (centre), and its structure in the poloidal plane (right), are shown.

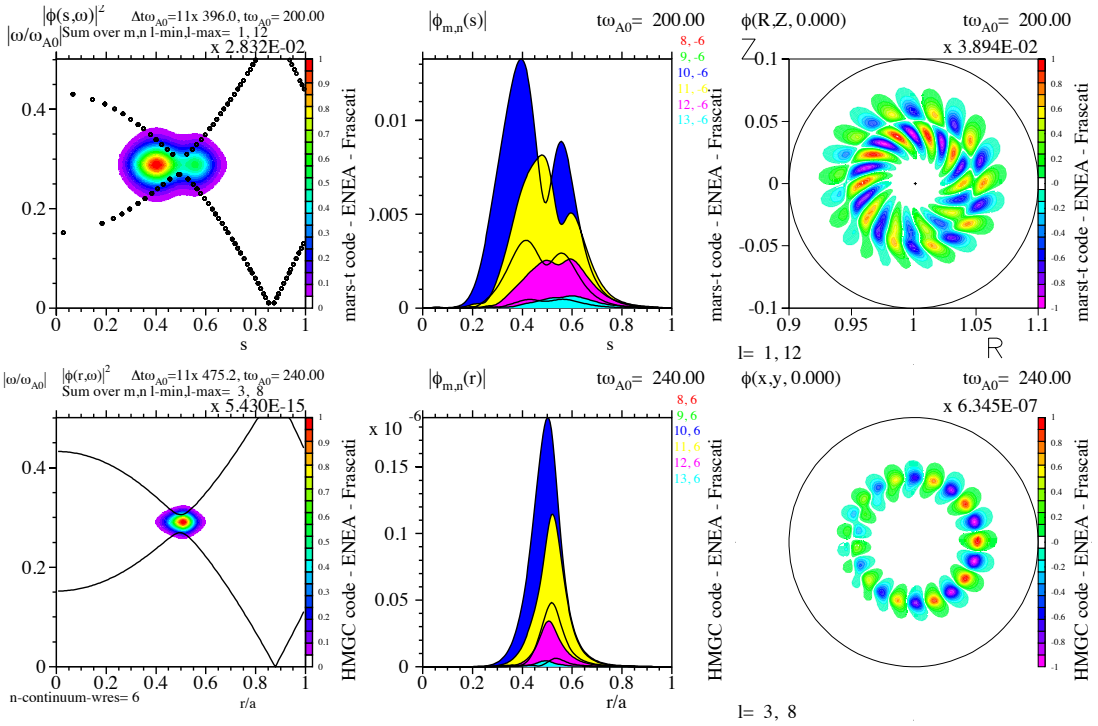


**Figure 14.** Test case B: results from HYMAGYC (top) and HMGC (bottom) for $n_{H0}/n_{i0} \approx 7.2\times10^{-3}$. The frequency spectrum of the fluctuating electrostatic potential $\phi$ (left), its poloidal Fourier components (centre), and its structure in the poloidal plane (right), are shown.

of the mode in the poloidal plane is clearly observed (see Fig. 13, right top and bottom frames). Simulations performed with the mixed "hmgc-hymagyc" code show results very similar to the ones obtained with HMGC, and here are not shown. In the spirit of the ITPA benchmark, a set of simulations varying $T_H$ has been performed, changing, accordingly, $v_{H0}/v_{A0}$ and $\rho_{H0}/a$; to perform this exercise, we have chosen a lower value of $n_{H0}/n_{i0}$ (w.r.t. the reference ITPA benchmark case), in order to compare the two codes in a regime were both observe the same mode, i.e., the TAE, as the most unstable mode ($n_{H0}/n_{i0} = 2.\times10^{-3}$). Figure 15 shows the growth rate vs. $T_{H0}$ for HYMAGYC and HMGC, and, also, for the value $T_{H0} = 400$ keV, the EP drive $\gamma_{drive}$, as obtained by algebraically subtracting from the growth rate the damping estimated by extrapolating to $n_{H0}/n_{i0} = 0$ the growth rates from Fig. 12, left (similarly to what was shown in Fig. 1 of Ref. [39]): the relative difference between the $\gamma_{drive}$ as obtained by HYMAGYC and HMGC is, indeed, reduced w.r.t. the one of the growth rates, as already found for the benchmark case A. Taking into account that simulations performed with the mixed "hmgc-hymagyc" code show results very similar to the ones obtained by HMGC, we can infer that the observed differences between HMGC and HYMAGYC simulations (namely, the symmetry in the poloidal plane of the TAE mode (Fig. 13) and the quantitative discrepancy of the growth rates (Fig. 15) at low-density EP values; and the different most unstable mode observed at high-density EP values - a TAE by HMGC

and a KTAE by HYMAGYC) could be ascribed to the differences of the MHD modules used in the two codes.

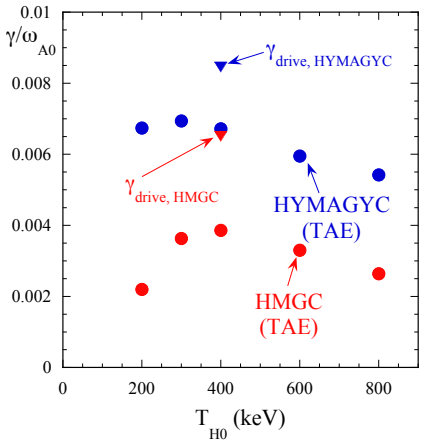


**Figure 15.** Test case B: normalized growth rates versus $T_{H0}$ at $n_{H0}/n_{i0} = 2. \times 10^{-3}$. Results for HMGC (red symbols) and HYMAGYC (blue symbols) simulations are shown; the triangles at $T_{H0} = 400$ keV are the EP $\gamma_{drive}$.

## 4. Conclusions

In summary, an extensive linear benchmark exercise has been performed between the hybrid MHD gyrokinetic codes HYMAGYC and HMGC in the limit of validity of the HMGC code (small aspect ratio, circular cross section, $k_\perp \rho_H \ll 1$, zero bulk pressure). Two equilibria have been considered (one of them, the test case B, being the so-called ITPA-TAE test case) and the two codes have been compared both in the MHD limit and in a wide range of the EP parameter space. In particular, in the test case A, frequencies, growth rates, spatial structures of the unstable modes ("Upper mode" and/or EPM) have been compared varying independently the EP density, thermal velocity and Larmor radius. The two codes manifest the same trends w.r.t. the variation of the parameters and to the occurrence of the EPM to become dominant. Some quantitative differences regarding the growth rates have been observed; nevertheless, by extracting the damping contribution from the growth rates, the EP drives, $\gamma_{drive}$, have been obtained and the agreement between HYMAGYC and HMGC improves considerably. Regarding the test case B, a rich MHD spectrum obtained by the eigensolver MARS has been presented. In the presence of EP drive, the two codes behave similarly for small values of EP density, showing a TAE as the most unstable mode. For higher values of EP density, HYMAGYC shows a stronger mode emerging from the lower Alfvén continuum as the most unstable one, whereas HMGC still observes a TAE. In the range of EP density where both codes observe the TAE, the trend of the growth rate w.r.t. $T_H$, as found

by HYMAGYC and HMGC, is similar, and the agreement improves when considering the contribution of the EP drive to the growth rate, $\gamma_{drive}$. The main discrepancies observed can be traced back to the different response of the MHD solvers, e.g., w.r.t. continuum damping and discretization schemes. In particular these differences can be more relevant for the test case B, which is characterized by a very low magnetic shear equilibrium.

In order to fully exploit the HYMAGYC potentialities, we plan for the near future to relax the constraints used in the present paper, investigating the finite Larmor radius and magnetic compression effects in realistic (e.g., shaped) equilibria, both in linear and nonlinear regimes.

## Acknowledgments

Part of the computing resources and the related technical support used for this work have been provided by CRESCO/ENEAGRID High Performance Computing infrastructure and its staff [40], and part by the EUROfusion Gateway Cluster hosted by IPP Garching. This work has been carried out within the framework of the EUROfusion Consortium and has received funding from the Euratom research and training programme 2014-2018 under grant agreement No 633053. The views and opinions expressed herein do not necessarily reflect those of the European Commission.

## References

[1] C.Z. Cheng, L. Chen, M.S. Chance, *Ann. Phys.*, 161 21, 1985.
[2] C.Z. Cheng, M.S. Chance, *Phys. Fluids*, 29 3695, 1986.
[3] R.R. Mett, S.M. Mahajan, *Phys. Fluids B*, 4 2885, 1992.
[4] L. Chen, Phys. Plasmas 1 1519, 1994.
[5] K.-L. Wong, *Plasma Phys. Control. Fusion*, 41 R1-R56, 1999.
[6] B.N. Breizman, S.E. Sharapov, *Plasma Phys. Control. Fusion*, 53 054001, 2011.
[7] ITER Physics Basis *Nucl. Fusion*, 39 2137-664, 1999.
[8] A. Fasoli et al. *Nucl. Fusion*, 47 S264, 2007.
[9] D.A. Spong, B.A. Carreras, and C.L. Hedrick, *Phys. Fluids B*, 4 3316, 1992.
[10] C.Z. Cheng, *Phys. Rep.*, 211 1, 1992.
[11] A.B. Mikhailovskii, G.T.A. Huysmans, S.E. Sharapov and W.O. Kerner, *Plasma Phys. Rep.* 23 844, 1997.
[12] S.D. Pinches et al. *Comput. Phys. Commun.*, 111 131, 1998.
[13] N.N. Gorelenkov, C.Z. Cheng and G.Y. Fu, *Phys. Plasmas*, 6 2802, 1999.
[14] D. Borba et al., *Nucl. Fusion*, 42 1029-1038, 2002.
[15] Y.Q. Liu, M.S. Chu, I.T. Chapman and T.C. Hender, *Phys. Plasmas*, 15 112503, 2008.
[16] L.J. Zheng, M.T. Kotschenreuther and J.W. Van Dam, *J. Comput. Phys.*, 229 3605, 2010.
[17] W. Park et al., *Phys. Fluids B*, 4 2033, 1992.
[18] S. Briguglio, G. Vlad, F. Zonca, and C. Kar. *Physics of Plasmas*, 2:3711-3723, 1995.
[19] Y. Todo, T. Sato, K. Watanabe, T.H. Watanabe and R. Horiuchi, *Phys. Plasmas*, 2 2711, 1995.
[20] S. Briguglio, F. Zonca, and G. Vlad. *Physics of Plasmas*, 5:3287-3301, 1998.
[21] Y. Todo and T. Sato, *Phys. Plasmas*, 5 1321, 1998.
[22] W. Park, E.V. Belova, G.Y. Fu, X.Z. Tang, H.R. Strauss and L.E. Sugiyama, *Phys. Plasmas* 6 1796, 1999.

[23] Y. Todo, K. Shinohara, M. Takechi and M. Ishikawa, *Phys. Plasmas*, 12 012503, 2005.
[24] Y. Todo, *Phys. Plasmas*, 13 082503, 2006.
[25] X. Wang, S. Briguglio, L. Chen, C. Di Troia, G. Fogaccia, G. Vlad and F. Zonca, *Phys. Plasmas*, 18 052504, 2011.
[26] Michael Cole, Alexey Mishchenko, Axel Knies, Ralf Kleiber, and Matthias Borchardt *Phys. Plasmas* 21 072123, 2014.
[27] A. Mishchenko, A.Könies, and R. Hatzky, *Phys. Plasmas*, 16 no.8 082105, 2009.
[28] W. Deng, Z. Lin, I. Holod, X. Wang, Y. Xiao and W. Zhang, *Phys. Plasmas*, 17 112504, 2010.
[29] M.D.J. Cole, A. Mishchenko, A. Könies, R. Hatzky and R. Kleiber, *Plasma Phys. Control. Fusion*, 57 054013, 2015.
[30] A.J. Brizard and T.S. Hahm, *Rev. Mod. Phys.*, 79 421-468, 2007.
[31] G. Vlad, S. Briguglio, G. Fogaccia, and F. Zonca. In *11th IAEA Technical Meeting on Energetic Particles in Magnetic Confinement Systems, Kyiv 21-23 Sept. 2009*, pages P-25, Vienna, Austria, 2009. International Atomic Energy Agency.
[32] H. Lütjens, A. Bondeson and O. Sauter. *Comput. Phys. Commun.* 97:219-260, 1996.
[33] F. Imbeaux et al. *Comp. Phys. Comm.* 181(6):987-998, 2010
[34] A. Bondeson, G. Vlad, and H. Lütjens. In *IAEA Technical Committee Meeting on Advances in Simulations and Modelling of Thermonuclear Plasmas, Montreal, 1992*, page 306, Vienna, Austria, 1993. International Atomic Energy Agency.
[35] G. Vlad, F. Zonca, and S. Briguglio. *Rivista del Nuovo Cimento*, 22(7):1-97, 1999.
[36] A. Bondeson and G.Y. Fu. *Comput. Phys. Comm.* 66:167-176, 1991.
[37] E.A. Frieman and L. Chen, *Phys. Fluids*, 25 502, 1982.
[38] G. Fogaccia, S. Briguglio, and G. Vlad. In *40th European Physical Society Conference on Plasma Physics, Espoo, Finland, 1st - 5th July 2013*, volume 37D, page P4.151. European Physical Society, 2013.
[39] A. Könies et al. In *Fusion Energy 2012*, Vienna, 2012. International Atomic Energy Agency. Paper 437-ITR/P1-34.
[40] G. Ponti et al. *Proceedings of the 2014 International Conference on High Performance Computing and Simulation, HPCS 2014*, art. no. 6903807, 1030-1033.